Available online at www.sciencedirect.com

SciVerse ScienceDirect

Ceramics International 39 (2013) 2551–2559

CERAMICS INTERNATIONAL

www.elsevier.com/locate/ceramint

Some studies on nucleation, crystallization, microstructure and mechanical properties of mica glass-ceramics in the system $0.2BaO \cdot 0.8K_2O \cdot 4MgO \cdot Al_2O_3 \cdot 6SiO_2 \cdot 2MgF_2$

Amit Mallik, Arunabha Basumajumdar*, P. Kundu, P.K. Maiti

Department of Chemical Technology, University of Calcutta, 92 A.P.C. Road, Kolkata 700009, India

Received 16 July 2012; received in revised form 31 August 2012; accepted 5 September 2012
Available online 13 September 2012

Abstract

The crystallization, microstructure, microhardness and theoretical machinability have been investigated by DTA, XRD, SEM and Microhardness Indenter of resulting glass-ceramics. Two distinct crystallization exotherms in the DTA curve are observed and resolved. The first peak corresponds to the initial formation of potassium fluorophlogopite and the second is due to the formation of barium fluorophlogopite. The activation energy for precipitation of each crystalline phase has been evaluated, and the crystallization mechanism has been studied. DTA analyses were conducted at different heating rates and the activation energy was determined graphically from Kissinger and Ozawa equation. The average activation energy is calculated as 276 KJ/mol for the first and 366 KJ/mol for the second crystallization peak. The Avrami exponent for first and second crystallization peak temperature determined by Augis and Bennett method is found to be 3 and 3.9, respectively. The results indicate that the growth of mica is a two and three dimensional process, controlled by the crystal-glass interface reaction. The Vicker's hardness decreased steadily at intermediate heat treatment temperature with the formation of barium and potassium fluorophlogopite phase, but the decrease in hardness is more rapid at higher temperature with the development of an interconnected 'house of cards' microstructure.

Keywords: B. Microstructure-final; D. Glass ceramics; Crystallization; Machinability

1. Introduction

Machinable glass-ceramics, wherein two-dimensional mica crystals are nucleated internally and crystallized from fluorine containing glasses have been developed [1], which can be machined to precise tolerances and surface finish with conventional metal working tools. Beall [1] first undertook the studies of the alkaline earth fluormica glass-ceramics. Later on Hoda and Beall [2] investigated different glass compositions containing barium, calcium, and strontium close in composition to the respective fluorophlogopite stoichiometry. Most of the compositions were susceptible to crystallization during casting. Only a few stoichiometric compositions were investigated and despite offering improved mechanical and dielectric strength, no further studies exist in the literature where compositional details are given. Henry and Hill [3,4], have shown that reduction in alumina content reduces the glass transition temperature, first crystallization peak temperature and promotes bulk crystal nucleation. The glasses with high alumina contents gave rise to feathery microstructures that did not coarsen readily to give blocky crystals of high aspect ratio and therefore could not produce the classic 'house of cards' microstructure. Hardness and machinability were found to be highly dependent on the formation of an interconnected 'house of cards' microstructure.

Greene et al. [5] investigated the $(1-Z)$ BaO: Z K_2O: (6–X) MgO: X MgF_2:(3–Q) Al_2O_3: Q B_2O_3: $8SiO_2$ system (where $Z=0$, 0.25, 0.5, 0.75 and 1.0, $X=2$, 2.5 and 3.0 and $Q=0$, 0.5 and 1) and observed that the substitution of

*Corresponding author. Tel.: +91 33 2351 9755; fax: +91 94 33 459 595.
E-mail address: a.basumajumdar@gmail.com (A. Basumajumdar).

0272-8842/$ - see front matter © 2012 Published by Elsevier Ltd and Techna Group S.r.l.
http://dx.doi.org/10.1016/j.ceramint.2012.09.015

barium by potassium results in increase in molar volume and co-efficient of thermal expansion and decrease in fractional glass compactness, microhardness and glass transition temperature values.

In the earlier work [6], authors had studied the kinetics as well as the crystal growth with respect to fluorine content in the barium fluorophlogopite glass-ceramics based on the system $BaO \cdot 4MgO \cdot Al_2O_3 \cdot 6SiO_2 \cdot 2MgF_2$, where it was indicated that the crystallization of the glass was largely homogenous and fluorine promotes initial crystallization.

Authors [7] had studied the kinetics as well as crystallization behavior, microstructure and mechanical properties of the system $Ba_x \cdot K_{1-2x} \cdot Mg_3 \cdot Al \cdot Si_3 \cdot O_{10} \cdot F_2$ ($x=0.0$, 0.3 and 0.5), where it was indicated that machinability and strength can be customized by judicious substitution of potassium by barium and also by the duration of heat treatment schedule.

It can be noted from above work that there is further scope of study for the improvement of machinability and hardness. In order to achieve the improvement of above properties, the present work has been undertaken wherein we have studied the crystallization, microstructure and mechanical behavior of $Ba_{0.1} \cdot K_{0.8} \cdot Mg_3 \cdot Al \cdot Si_3 \cdot O_{10} \cdot F_2$ glass.

2. Experimental

2.1. Glass synthesis and ceramisation

Analytical grade chemicals in powder form were used as starting materials in this study. The powders were from Merck Specialties Private Limited, India. The weight percentage chemical composition of the glass is BaO 3.59, K_2O 8.82, MgO 18.87, Al_2O_3 11.93, SiO_2 42.20, MgF_2 14.59. An overall 2.00 weight percentage of B_2O_3, was added purposefully to reduce the viscosity and thereof to increase the rate of diffusion of different ionic species in glass, which may result in the natural tendency towards directional growth of crystals [8]. The glass batches were properly mixed in an attrition mill thereafter melted in a platinum crucible for 4 to 5 h in an electrically heated furnace operating at 1450–1500 °C with occasional stirring with a glass rod (quartz) in order to achieve the homogeneity of the molten glass. After the melting operation is over, the molten mass was poured into a preheated cast iron mold to make rectangular slabs of dimension 50 mm × 25 mm × 10 mm. Immediately after casting, the prepared rectangular slabs of glass samples were released from the mold and were quickly introduced into an annealing furnace operating at 650 °C and soaked for 1 h followed by natural cooling to room temperature.

After annealing, the block was cut into pieces to about 1–2 mm thickness with the help of a precision low speed cutting machine (Buehler). These cut samples were fired at 680 °C for 2 h for nucleation. This nucleation temperature was determined by Differential Thermal Analysis (DTA) study. Samples after nucleation were then heated to various crystallization temperatures (800, 900, 1000, 1100 and 1150 °C) at a rate of 2 °C/min and the samples were kept at the crystallization temperatures for 5 h.

2.2. Characterization techniques

2.2.1. Differential thermal analysis (DTA)

The DTA measurements were performed using Shimadzu DT40 thermal analyzer with α-alumina powder as a reference material. In this work, non-isothermal experiments of finely powdered samples (~200 μm) of about 17 mg placed in a platinum crucible were carried out at different heating rates (5, 10, 15 and 20 °C/min.) from ambient temperature to 1000 °C. Analytical models developed independently by Kissinger and Ozawa were used to analyze the DTA data and to determine the activation energy for crystallization. Avrami exponent was calculated by Augis and Bennett's equation.

2.2.2. X-ray powder diffraction (XRD)

X-ray powder diffraction experiment was carried out for the samples heat treated according to the schedule as described above. The ceramised glass samples were ground to ~75 μm. XRD experiments were performed by an X-ray powder diffractometer (PW 1830, Panalytical) using Ni filtered Cu-k_α X-radiation with scanning speed of 2°(2θ)/ min. The diffraction pattern was recorded within Bragg's angle ranges $5° < 2\theta < 70°$. The phases were identified by JCPDS numbers (ICDD-PDF2 data base).

2.2.3. Scanning electron microscopy (SEM)

Different samples heated at the crystallization temperatures according to the schedule mentioned before were studied to investigate the development of microstructure with back scattered electron imaging (BEI) mode in a Hitachi, S3400N, Japan, scanning electron microscope. Before microstructural study, surface of all the samples were polished by following standard procedures and finally with diamond paste. The polished samples for scanning electron microscopy were prepared by etching for 1/2 min with an aqueous solution of 5% NaOH and 1% EDTA at about 80 °C.

2.2.4. Vicker's hardness

For this study, glass ceramic samples were mounted on resin and after curing, the samples were finely polished. The indenter was pressed onto the polished surface of the material at a load of 500 g with a dwelling time of 15 s.The size of the impression was measured using LEITZ microhardness indenter. The machine used was carver press. The Vicker's number (H_V) is calculated using the following formula [9]:

$$H_V = 1.854 \frac{P}{D^2} \quad (1)$$

where, P=applied Load (measured in kilogram-force) and; D=length of the diagonal of the indentation (measured in millimeter).

The hardness value was measured for samples of different batches heat treated at different temperatures.

To convert the Kg/mm^2 to GPa the following relation was used

$$H_V(\text{GPa}) = \frac{9.81}{1000} \times H_V \quad (\text{Kg/mm}^2) \tag{2}$$

2.2.5. Machinability

Machinabilty is an important tool to characterize machinable glass-ceramics. As such it is very much essential to measure or calculate the machinabilty or the machinabilty parameter of such materials. The following equation indicates the relationship between hardness (H_v) and machinability parameter (m) [10].

$$m = 0.643 - 0.122 H_V \tag{3}$$

2.2.6. Fracture toughness

The fracture toughness of a material is determined from the stress intensity factor at which the crack will propagate and lead to fracture. It can be calculated from the size of the crack developed during Vicker's hardness testing by using the following formula [11,12].

$$K_{IC} = 0.025 \frac{P}{C^{1.5}} \tag{4}$$

where, C is the average crack length in mm; P is the applied load (measured in kilogram-force).

2.2.7. Modulus of rupture

Rectangular bar specimens, ground and polished with 3 μm, 1 μm and 0.5 μm diamond paste were broken in three-point bending tests (span length, 15 to 20 mm) at a crosshead speed of 0.5 mm/min using Instron 4411 flexural testing machine. The flexural strength represents the highest stress experienced within the material at its moment of rupture [13,14]. It is measured in terms of stress.

The MOR of a rectangular sample under a load in a three-point bending setup is

$$\sigma = \frac{3FL}{2bd^2} \tag{5}$$

where, F is the load (force) at the fracture point; L is the length of the support span; b is width; d is thickness.

3. Result and discussion

3.1. Kinetics of crystallization

DTA curves for glass samples at a heating rate of 5, 10, 15 and 20 °C/min are shown in Fig. 1. Two well-defined crystallization peaks are visible in all the DTA thermograms. When the glass sample was heated at 10 °C/min, the 1st peak appeared at 762 °C and the 2nd peak appeared at 858 °C [6,15]. Moreover, it is clear from these curves that the two distinct crystallization peak temperatures shifted towards right with increasing heating rate.

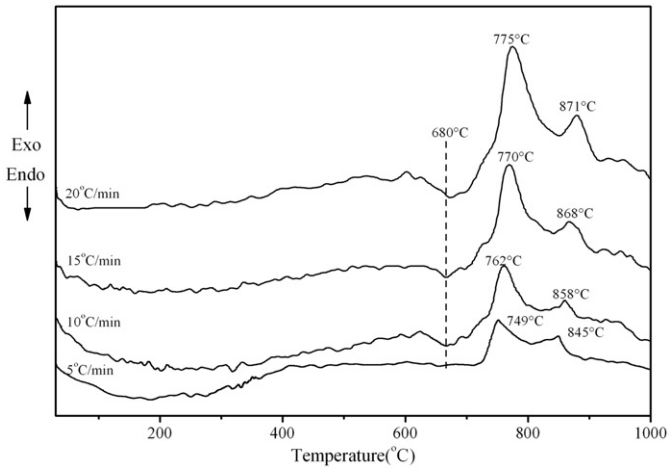

Fig. 1. Differential thermal analysis plots of glass samples of varying heating rate: (1) 5 °C/min, (2) 10 °C/min, (3) 15 °C/min, (4) 20 °C/min.

The nucleation and crystallization temperatures were determined from DTA analysis of the glass sample.

The isothermal kinetics of glass crystallization is studied on the basis of the Jonhson–Mehl–Avrami (JMA) equation [16–21].

$$x = 1 - exp\,[-(kt)^n] \tag{6}$$

where x is the volume fraction crystallized at a given temperature during time t; k is the reaction rate constant and n is the Avrami exponent, which is a dimensionless factor depending on the nucleation process and growth morphology.

Based on Jonshon–Mehl–Avrami equation, non-isothermal crystallization kinetics of glass can be described by the Kissinger and Ozawa equation [22–25].

Kissinger equation:

$$\ln \frac{T_p^2}{\beta} = \frac{E}{RT_p} + C \tag{7}$$

Ozawa equation:

$$\ln \beta = -\frac{E}{RT_p} + C \tag{8}$$

where T_p is the crystallization peak temperature in a DTA curve, β is the heating rate, E is the activation energy of crystal growth, R is the universal gas constant and C is constant.

Using Kissinger Eq. (7), ln (T_p^2/β) was plotted against $1/T_p$ and the slope of the plot is equal to E/R (Fig. 2a and b), from which E can be calculated. Similarly using Ozawa Eq. (8), ln β was plotted against $1/T_p$ and the slope of the plot is equal to E/R (Fig. 2c and d), from which E can be calculated. The values of activation energy are given in Table 1.

From Augis–Bennett equation [26], the value of Avrami exponent (n) can be estimated using the value of activation energy

$$n = \frac{2.5}{\Delta T} \times \frac{RT_p^2}{E} \tag{9}$$

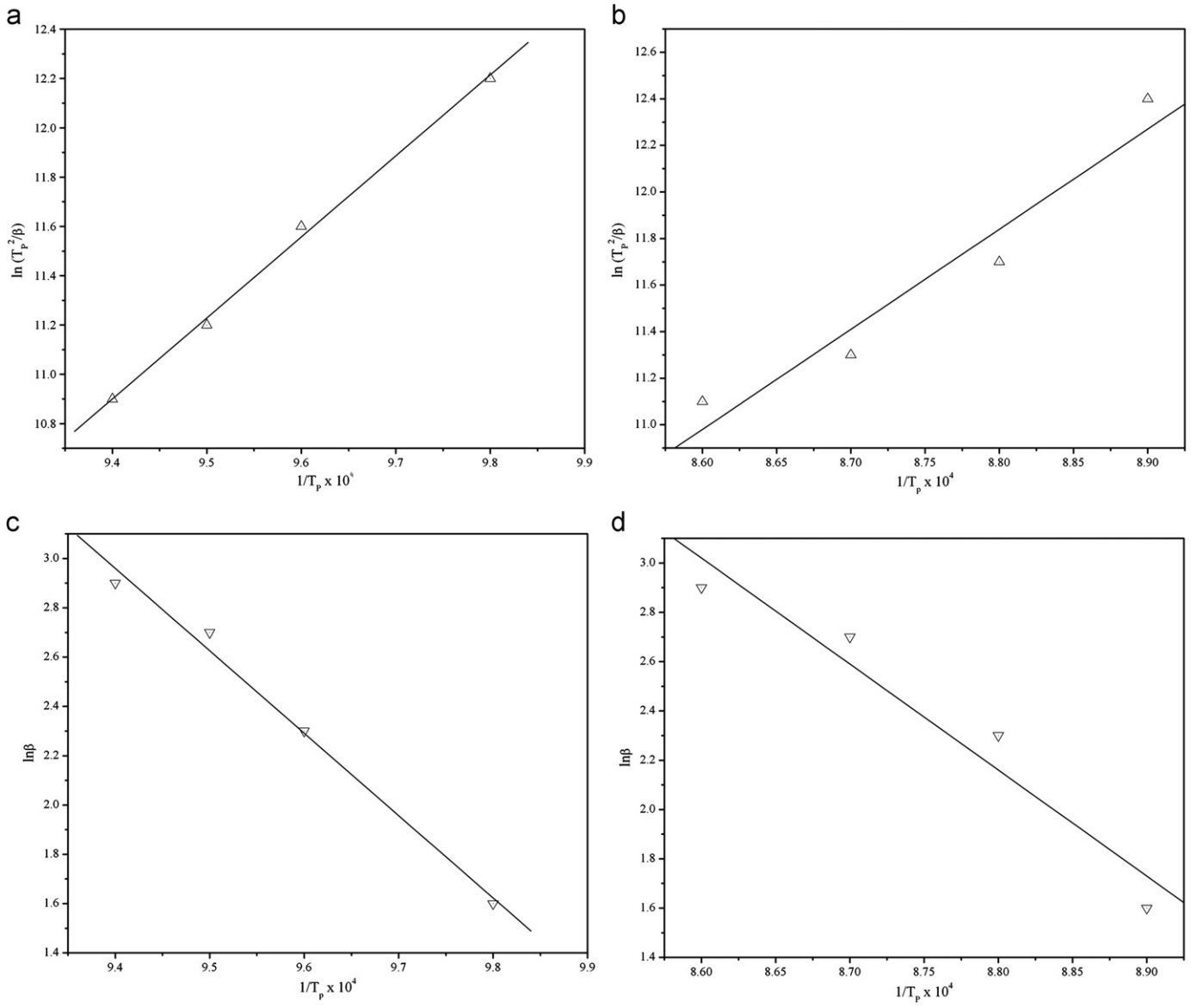

Fig. 2. (a) Kissinger plot of ln (T_P^2/β) against $1/T_p$ at 1st crystallization peak temperature (T_p^1). (b) Kissinger plot of ln (T_P^2/β) against $1/T_p$ at 2nd crystallization peak temperature (T_p^2). (c) Ozawa plot of lnβ against $1/T_p$ at 1st crystallization peak temperature (T_p^1). (d) Ozawa plot of lnβ against $1/T_p$ at 2nd crystallization peak temperature (T_p^2).

Table 1
Values of activation energy (Kissinger equation [E_K]+Ozawa equation [E_O]) and Avrami exponent.

Heating rate (β) (K/min)	1st crystallization temperature (T_p^1) (K)						2nd crystallization temperature (T_p^2) (K)					
	T_p^1	Activation energy (KJ/mol)		$<E>$ (KJ/mol)	Avrami exponent (n)	$<n>$	T_p^2	Activation energy (KJ/mol)		$<E>$ (KJ/mol)	Avrami exponent (n)	$<n>$
		Kissinger (E_k)	Ozawa (E_o)					Kissinger (E_k)	Ozawa (E_o)			
5	1022	273.1	277.9	275.5	2.70	2.89	1118	357.5	374.1	365.8	3.60	$3.88 \approx 4.00$
10	1035				2.82	≈ 3.00	1131				3.85	
15	1043				2.90		1141				3.95	
20	1048				3.12		1144				4.10	

where, n is the Avrami exponent or crystallization index and ΔT is the full width of the exothermic peak at half-maximum intensity. The values of Avrami exponent are given in Table 1. The crystallization index (n) depends upon the actual nucleation and growth mechanism. According to JMA theory, crystallization index (n) depends on the crystallization manner,

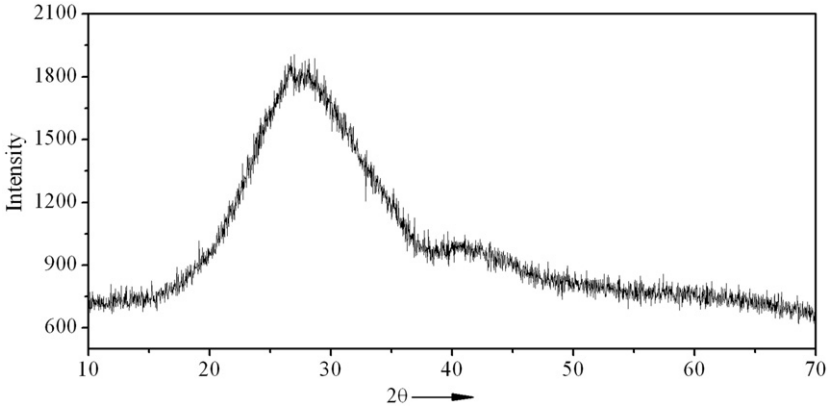

Fig. 3. XRD patterns for glass samples.

Table 2
List of JCPDS files used to identify the main crystal phase formations observed.

Crystal phase	JCPDS reference file
Barium fluorophlogopite ($Ba_{0.5} \cdot Mg_3 \cdot Al \cdot Si_3 \cdot O_{10} \cdot F_2$)-BF	16-344*
Potassium fluorophlogopite ($K \cdot Mg_3 \cdot Al \cdot Si_3 \cdot O_{10} \cdot F_2$)-KF	01-076-0816
Alpha-hexacelsian ($Ba_{0.808}$ ($Al_{1.}71 \cdot Si2_{29}) \cdot O_8$)-H	01-088-1050
Enstatite ($MgSiO_3$)-E	00-002-0546

*Ref. [2]

$n \cong 2$ means that the surface crystallization dominates overall crystallization, $n \cong 3$ means that the two dimensional crystallization or volumetric crystallization, $n \cong 4$ means that the three dimensional crystallization for bulk materials [27–30].

3.2. X-ray diffraction

The synthesized glass samples are characterized by XRD and the samples are found to be amorphous, which was confirmed by a broad spectrum obtained in XRD pattern (Fig. 3). In order to understand the nucleation and crystallization kinetics these glasses were crystallized at different temperatures (800, 900, 1000, 1100 and 1150 °C) for a duration of 5 h keeping the nucleation temperature (680 °C) and time 2 h for all samples. It is needless to mention that the nucleation temperatures were calculated for the batch from DTA thermogram at a heating rate of 10 °C/min.

The JCPDS reference files used to identify the various crystal phases are presented in Table 2. The appearance of K-fluorophlogopite and Ba-fluorophlogopite are observed in all heat treated samples (Fig. 4). At 800 °C, several peaks of K-fluorophlogopite appeared as major phase and Ba-fluorophlogopite and alpha-hexacelsian appeared as minor phase. At 900 °C, additional peaks of Ba-fluorophlogopite and K-fluorophlogopite appeared. At 1000 °C, further additional peaks of K-fluorophlogopite appeared and the appearance of enstatite as a new phase in the material is also confirmed.

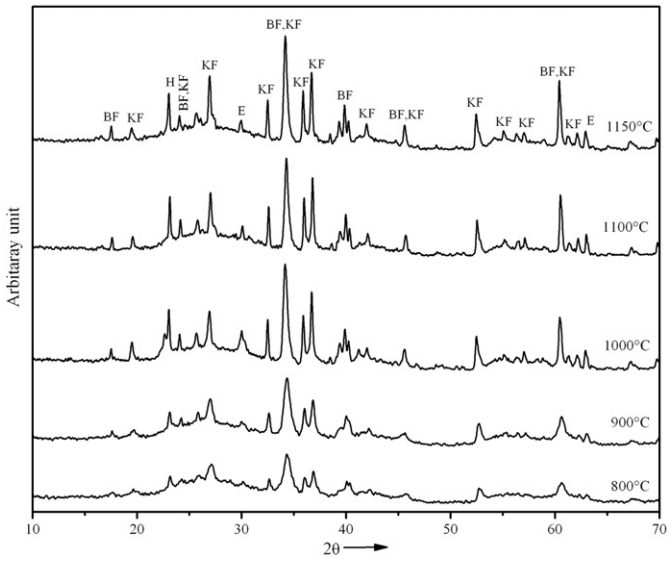

Fig. 4. XRD patterns for glass samples at different crystallization temperatures. (B-Barium fluorophlogopite, K-Potassium fluorophlogopite, H-Alpha-hexacelsian and E-Enstatite).

At 1100 °C, there is no change in the intensity of peaks except the appearance of new peaks of K-fluorophlogopite. Also, there is no change in the intensity of the peaks at 1150 °C whereas the sharpness of the peaks increases. With increasing heat treatment temperature, the number of peaks of K-fluorophlogopite is increased but the number of peaks of Ba-fluorophlogopite remains same. This may be an indication of the Ba-fluorophlogopite formation at lower temperature in this composition.

3.3. Microstructure analysis

Samples heated at 800 °C for 5 h, exhibit very fine submicron microstructures and consist of some blocky crystal (Fig. 5a). But when the samples were heated at 900 °C for 5 h, they exhibited a large number of slightly bigger blocky crystals (Fig. 5b) compared to that at 800 °C. These crystals are dense and appeared white in the back scattered electron micrographs with more or less

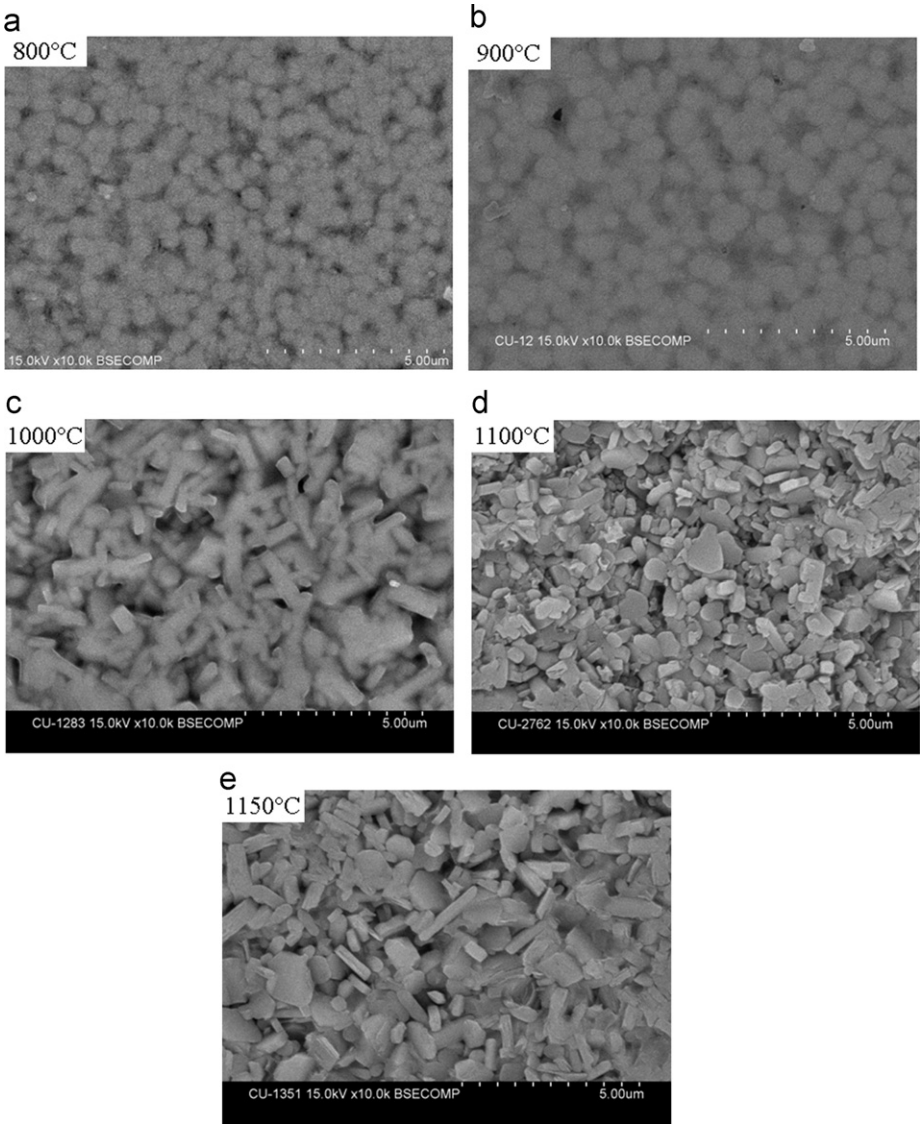

Fig. 5. SEM photographs of polished and etched surface of samples nucleated at 680 °C for 2 h and ceramised for 5 hr at (a) 800 °C, (b) 900 °C, (c) 1000 °C, (d) 1100 °C and (e) 1150 °C.

low aspect ratio in highly siliceous residual glass with acicular morphology.

Samples heated at 1000 °C for 5 h exhibited the appearance of lath like crystals with acicular morphology (Fig. 5c).

Samples heated at 1100 °C for 5 h exhibited the appearance of large sized crystals with acicular morphology (Fig. 5d). But the sample heated at 1150 °C for 5 h, exhibits the development of large sized crystals with acicular morphology and forms "house of cards" structures (Fig. 5e).

The appearance of blocky crystals might be due to the formation of mica booklets and in many cases have an aspect ratio (length/diameter) of <1. As the temperature further increased, the number of crystal per unit volume decreased and aspect ratio of the crystal increased (Fig. 5a and b). It might be due to the dissolution of crystals with an aspect ratio of <1 and reprecipitation of constituents onto those crystal of higher aspect ratio. This energetically unfavorable configuration might therefore be the driving force towards attaining the long crystal observed after heat treatment for 5 h at 1000 °C, 1100 °C and 1150 °C (Fig. 5c, d and e), which has been discussed by Chyung et al. [31].

3.4. Vicker's hardness (H_v), machinability (m), fracture toughness (K_{IC}) and modulus of rupture (MOR)

It is observed that at 800 °C, the Vicker's hardness value reduces to a large extent on the formation of either potassium or barium fluorophlogopite, or both of potassium and barium fluorophlogopite phases compared to that of original glass (Table 3).

When the temperature is progressively increased, the Vicker's hardness values gradually decrease upto 1100 °C. The hardness values increase slightly when heated beyond this temperature to 1150 °C (Fig. 6), but this increased value is very low compared to the original glass (Table 3). The large reduction in hardness value correlates with the

Table 3
Microstructural analysis of different heat-treated samples.

Heat treatment temperature	Vickers hardness (H_v) in GPa	Fracture toughness (K_{IC}) $\times 10^3$ in MPa $m^{1/2}$	Machinability parameter (m)	Modulus of rupture (MOR) in MPa
Glass	7.19	18.2	−0.234	108.8
800 °C	4.31	12.5	0.117	205.8
900 °C	4.02	11.8	0.153	245.7
1000 °C	3.71	11.1	0.190	279.5
1100 °C	3.31	10.2	0.239	309.9
1150 °C	3.54	10.7	0.211	262.4

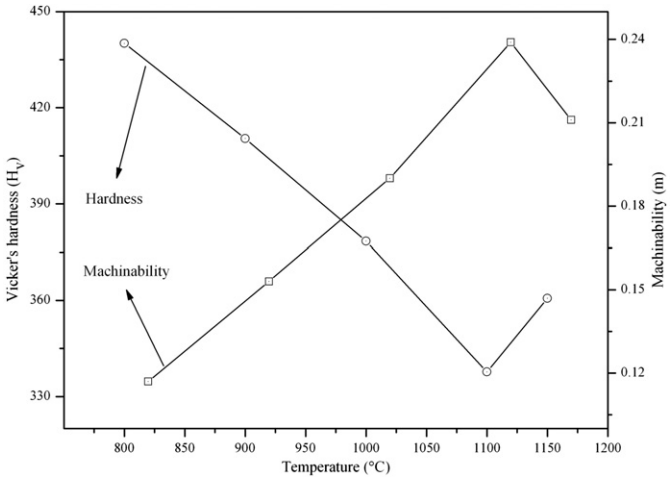

Fig. 6. Vicker's hardness (H_v) and machinability (m) against different heat treatment temperatures.

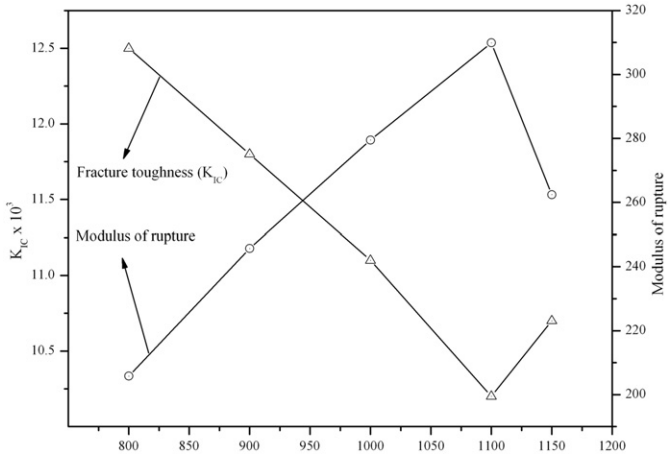

Fig. 7. Fracture toughness (K_{IC}) and modulus of rupture (MOR) against different heat treatment temperatures.

formation of the interconnected "house of cards" microstructure [32–37]. At any particular temperature, the hardness values increase with gradual increase in barium content.

The machinability parameter has been calculated from Vicker's hardness (H_v) values and is shown in Fig. 6. It is clear from Fig. 6 and Table 3 that the higher the hardness values, the lower the machinability parameter [38,39]. The fracture toughness has been calculated from Vicker's hardness (H_v) values, and is shown in Fig. 7. It is clear from Fig. 7 and Table 3 that higher the hardness values, higher are the fracture toughness. At any particular temperature, the fracture toughness increases with gradual increase in barium content. Invariably in this batch, crystallized at 1150 °C, the sudden increase in hardness values may be due to the formation of other crystal phases like enstatite and barium aluminum silicate etc.

At 800 °C, the modulus of rupture values increase to a large extent on the formation of either potassium or barium, or both of potassium and barium fluorophlogopite phases compared to those of original glasses. When the temperature is further increased, the modulus of rupture values gradually increase upto 1100 °C. The modulus of rupture values decrease slightly beyond this temperature at 1150 °C (Fig. 7), but the decrease is very low and is sufficiently higher than that of the original glasses [40]. The modulus of rupture of the glass-ceramics heated at 1150 °C was lower than that at 1100 °C because the barium fluorophlogopite and potassium fluorophlogopite crystals grew large (~5 μm), thereby probably introducing large sized critical flaws [41–45].

The hardness decreases with increasing aspect ratio of the crystal and the crystallinity of mica with simultaneous increase in the machinability. The glass-ceramics showing negative values of 'm' cannot be considered to be machinable, because they need a large threshold cutting force to initiate machining and are difficult to machine to intricate shapes also. On the other hand, samples having positive 'm' can be machined precisely by decreasing cutting speed with small cutting force [46,47]. Hardness, machinability and fracture toughness were found to be highly dependent on the formation of an interconnected 'house of cards' microstructures.

4. Conclusions

1. From XRD patterns, it can be concluded that at lower temperatures Ba-fluorophlogopite and K-fluorophlogopite are the major phases in the glass-ceramics. With increasing heat treatment temperature, other crystal phases viz. barium aluminum silicate (alpha-hexacelsian) and enstatite are also formed.
2. Partial substitution of potassium by barium in $K \cdot Mg_3 \cdot Al \cdot Si_3 \cdot O_{10} \cdot F_2$ system leads to the formation of K-fluorophlogopite and Ba-fluorophlogopite crystal phases simultaneously, and forms interconnected "house of cards" microstructure.
3. Hardness, machinability, fracture toughness and modulus of rupture were found to be highly dependent on the formation of an inter-connected "house of cards" microstructure and aspect ratio of the formed crystals.

Machinability and strength can be customized by judicious substitution of potassium by barium and also by the time of crystallization.

Acknowledgments

Financial support from University Grant Commission (UGC), under Major Research Project is gratefully acknowledged. SEM and XRD facility have been provided by technical education quality improvement programe. One of the authors, Amit Mallik thanks University Grant Commission (UGC), New Delhi, India, for providing junior research fellowship (RGNF).

References

[1] G.H. Beall, in: L.L. Hench, S.W. Frieman (Eds.), Advances Nucleation and Crystallization in Glasses, American Ceramic Society, Westerville, 1971, p. 251.
[2] S.N. Hoda, G.H. Beall, In: J.H. Simmons, D.R. Uhlmann (Eds.), Alkaline earth mica glass-ceramics, advances in ceramics: nucleation and crystallization in glasses, Journal of the American Ceramic Society 2 (1982) 287–300.
[3] J. Henry, R.G. Hill, Influence of alumina content on the nucleation crystallization and microstructure of barium fluorophlogopite glass-ceramics based on $8SiO_2 \cdot YAl_2O_3 \cdot 4MgO_2 \cdot MgF_2 \cdot BaO$. Part I. Nucleation and crystallization behavior, Journal of Materials Science 39 (2004) 2499–2507.
[4] J. Henry, R.G. Hill, Influence of alumina content on the nucleation crystallization and microstructure of barium fluorophlogopite glass-ceramics based on $8SiO_2 \cdot YAl_2O_3 \cdot 4MgO \cdot 2MgF_2 \cdot BaO$. Part II. Microstructure, microhardness and machinability, Journal of Materials Science 39 (2004) 2509–2515.
[5] K. Greene, M.J. Pomeroy, S. Hampshire, R. Hill, Effect of composition on the properties of glasses in the K_2O–BaO–MgO–SiO_2–B_2O_3–MgF_2 system, Journal of Non-Crystalline Solids 325 (2003) 193–205.
[6] P.K. Maiti, A. Mallik, A. Basumajumdar, P. Kundu, Influence of fluorine content on the crystallization and microstructure of barium fluorophlogopite glass-ceramics, Ceramics International 36 (2010) 115–120.
[7] P.K. Maiti, A. Mallik, A. Basumajumdar, P. Guha, Influence of barium oxide on the crystallization, microstructure and mechanical properties of potassium fluorophlogopite glass-ceramics, Ceramics International 38 (2012) 251–258.
[8] B.R. Lawn, D.B. Marshall, Hardness, toughness, and brittleness: an indentation analysis, Journal of the American Ceramic Society 62 (1979) 347–350.
[9] I.W. Donald, R.A. McCurrie, Microstructure and indentation hardness of an MgO–LiO_2–Al_2O_3–SiO_2–TiO_2 glass-ceramics, Journal of the American Ceramic Society 55 (1972) 289–291.
[10] G.A. Evans, E.A. Charles, Fracture toughness determinations by indentation, Journal of the American Ceramic Society 59 (1976) 371–372.
[11] I.M. Low, N. Duraman, J. Fulton, N. Tezuka, I.J. Davies, A comparative study of the microstructure-property relationship in human adult and baby teeth, Ceramic Engineering and Science Proceedings 26 (2005) 145–152.
[12] B.R. Lawn, M.V. Swain, Microfracture beneath point indentations in brittle solids, Journal of Materials Science 10 (1975) 113–122.
[13] B.R. Lawn, E.R. Fuller, Equilibrium penny-like cracks in indentation fracture, Journal of Materials Science 10 (1975) 2016–2024.
[14] P.K. Maiti, A. Mallik, A. Basumajumdar, K. Das, Some studies on nucleation, crystallization and microstructural behaviour of mica glass-ceramics in the system $0.8BaO \cdot 0.2K_2O \cdot 4MgO \cdot Al_2O_3 \cdot 6SiO_2 \cdot 2MgF_2$, Journal of Indian Chemical Society 88 (2011) 1509–1515.
[15] M. Avrami, Kinetics of phase change. i. General theory, Journal of Chemical Physics 7 (1939) 1103–1112.
[16] M. Avrami, Kinetics of phase change. ii. Transformation-time relations for random distribution of nuclei, Journal of Chemical Physics 8 (1940) 212–214.
[17] M. Avramim, Kinetics of phase change. iii. Granulation, phase change and microstructure, Journal of Chemical Physics 9 (1941) 177–184.
[18] J. Alton, T.J. Plaisted, Kinetics of growth of spinel crystals in a borosilicate glass, Chemical Engineering Science 57 (2002) 2503–2509.
[19] O. Grong, O.R. Myhr, Additivity and isokinetic behaviour in relation to diffusion controlled growth, Acta Materialia 48 (2000) 445–452.
[20] J.W. Cahn, The kinetics of grain boundary nucleated reactions, Acta Metallurgica 4 (1956) 449–459.
[21] J.W. Cahn, Transformation kinetics during continuous cooling, Acta Metallurgica 4 (1956) 572–575.
[22] H.E. Kissinger, Variation of peak temperature with heating rates in differential thermal analysis, Journal of Research of the National Bureau of Standard 57 (1956) 217–221.
[23] H.E. Kissinger, Reactions kinetics in differential thermal analysis, Analytical Chemistry 29 (1957) 1702–1706.
[24] T. Ozawa, Kinetics of non-isothermal crystallization, Polymer 12 (1971) 150–158.
[25] T. Ozawa, Temperature control modes in thermal analysis, Pure and Applied Chemistry 72 (2000) 2083–2099.
[26] J.A. Augis, J.E. Bennett, Calculation of the Avrami parameters for heterogeneous solid state reactions using a modification of the Kissinger method, Journal of Thermal Analysis 13 (1978) 283–292.
[27] K. Cheng, Evaluation of crystallization kinetics of glasses by non-isothermal analysis, Journal of Materials Science 36 (2001) 1043–1048.
[28] Y.J. Park, J. Heo, Nucleation and crystallization kinetics of glasses derived from incinerator fly ash waste, Ceramics International 28 (2002) 669.
[29] L.A. Perez-Maqueda, J.M. Criado, J. Malek, Combined kinetic analysis for crystallization kinetics of non-crystalline solids, Journal of Non-Crystalline Solids 320 (2003) 84–91Sol 320 (2003) 84–91.
[30] K. Matusita, S. Saka, Kinetic-study on crystallization of glass by differential thermal-analysis Criterion on application of Kissinger plot, Journal of Non-Crystalline Solids 39 (1980) 741–746.
[31] C.K. Chyung, G.H. Beall, D.G. Grossman, Fluorphlogopite mica glass-ceramics. In: Proceedings of the International Glass Congress, no. 14, Kyoto, Japan, Ceramic Society of Japan, (1974), pp. 33–40.
[32] A.C. Fischer-Cripps, Role of internal friction in indentation damage in a mica-containing glass-ceramic, Journal of the American Ceramic Society 84 (2001) 2603–2606.
[33] M. Goswami, A. Sarkar, T. Mirza, V.K. Shirkhande, Sangeeta, K.R. Gurumurthy, G.P. Kothiyal, Study of some thermal and mechanical properties of magnesium aluminium silicate glass-ceramic, Ceramics International 28 (2002) 585–592.
[34] S. Taruta, T. Hayashi, K. Kitajima, Preparation of Machinable cordierite/mica composite by low temperature sintering, Journal of the European Ceramic Society 24 (2004) 3149–3154.
[35] S. Taruta, R. Fujisawa, K. Kitajima, Preparation and mechanical properties of machinable alumina/mica composites, Journal of the European Ceramic Society 26 (2006) 1687–1693.
[36] A. Göel, D.U. Tulyaganov, V.V. Kharton, A.A. Yaremchenko, S. Agathopoulos, J.M.F. Ferreira, Effect of BaO addition on crystallization, microstructure and properties of diposide-Ca-Tschermak Clinopyroxene-based glass-ceramics, Journal of the American Ceramic Society 9 (2007) 2236–2244.
[37] G.H. Beall, Refractory glass-ceramics based on alkaline earth aluminosilicates, J. Euro. Ceram. Soc. 29 (2009) 1211–1219.
[38] T. Uno, T. Kasuga, S. Nakayam, Mechanical properties of Barium mica containing glass-ceramics, Journal of the European Ceramic Society 100 (1992) 315–319.
[39] V. Saraswati, S. Raoot, Machinable mica-based glass-ceramic, Journal of the Materials Science 27 (1992) 429–432.
[40] D.S. Baik, K.S. No, J.S. Chun, H.Y. Cho, Effect of the aspect ratio of mica crystals and crystallinity on the microhardness and machinablity of mica glass-ceramics, Journal of Materials Processing Technology 67 (1997) 50–54.

[41] A.R. Boccaccini, Machinablity and brittleness of glass-ceramics, Journal of Materials Processing Technology 65 (1997) 302–304.
[42] S. Habelitz, G. Carl, C. Russel, S. Thiel, U. Gerth, J.D. Schnapp, A. Jordanov, H. Knake, Mechanical properties of oriented glass-ceramic, Journal of Non-Crystalline Solids 220 (1997) 291–298.
[43] K.J. Anusavice, N.Z. Zhang, Effect of crystallinity and fracture toughness of $Li_2O \cdot Al_2O3 \cdot CaO \cdot SiO_2$ glass-ceramics, Journal of the American Ceramic Society 80 (1997) 1353–1358.
[44] K. Cheng, J. Wan, K. Liang, Enhanced mechanical properties of oriented mica glass-ceramics, Materials Letters 39 (1999) 350–353.
[45] T.J. Hill, J.J. Mecholsky, J.K. Anusavice, Fractal analysis of toughening behavior in $3BaO \cdot 5SiO_2$ glass-ceramics, Journal of the American Ceramic Society 83 (2000) 545–552.
[46] H.H.K. Xu, D.T. Smith, G.E. Schumacher, F.C. Eichmiller, J.M. Antonucci, Indentation modulus and hardness of whisker-reinforced heat-curved dental resin composites, Dental Materials 16 (2000) 248–254.
[47] P. Alizadeh, B.E. Yekta, A. Gervei, Effect of Fe_2O3 addition on the sinterability and machinability of glass-ceramics in the system $MgO \cdot CaO \cdot SiO_2 \cdot P_2O5$, Journal of the European Ceramic Society 24 (2004) 3529–3533.